APC 523 Final Project

Sihan Liu (MAE)

I. Introduction

The coexistence of multiple liquid phases is a widespread physical phenomenon in nature and industry. Examples include oil-in-water emulsions, beverages (cocktails), medicines, and cosmetic products, which are obtained by liquid-liquid phase separation [1]. In biology, cells are a typical multi-component liquid system in which thousands of distinct biomolecules interact with each other and perform various biological functions simultaneously [2]. There are numerous biomolecular condensates in cells that form through phase separation, such as nucleoli, stress granules, and P bodies [3-7]. These liquid-like organelles are rich in polymers including proteins and RNAs, and they compartmentalize the cell without the aid of membranes, thereby enabling spatiotemporal regulations of internal components and a range of biological processes [8-10]. In this project, we explore how to simulate the phase separation of multi-component liquid using a continuum model.

II. Equation for phase separation and the numerical method

The physics of phase separation can be characterized by the Flory-Huggins solution theory, in which the free energy density of the multi-component system is given by [11]

$$\overline{f} = \frac{f}{k_B T} = \sum_{i=1}^{N} \phi_i \ln \phi_i + \frac{1}{2} \sum_{i,j=1}^{N} \chi_{ij} \phi_i \phi_j - \frac{\lambda^2}{2} \sum_{i,j=1}^{N} \chi_{ij} \nabla \phi_i \cdot \nabla \phi_j$$

where ϕ_i is the volume fraction of component i, χ_{ij} is the Flory interaction parameter between components i and j, and λ is the characteristic width of the interface. The first term of the free energy density describes the entropic part, the second term indicates the intra-phase interaction, and the last term gives the interfacial energy. Phase separation occurs if χ_{ij} is large. For example, in a two-component system, the free energy density is changed by different χs, as shown in Fig. 1, and when $\chi > 2$, there are two minima, which means the solution can be stable with two different volume fractions and thus lead to phase separation. After phase separation, the solution will undergo morphology change in order to decrease the surface energy.

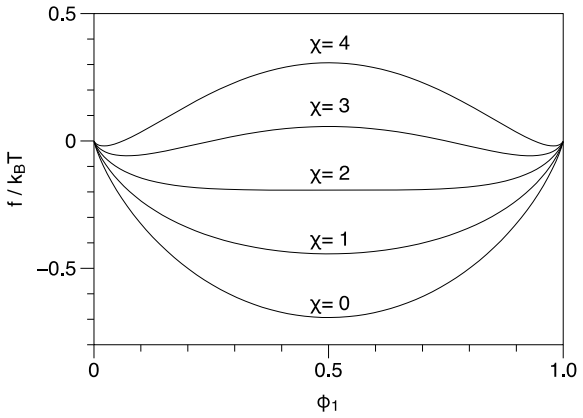

Fig. 1. Free energy density for a two-component system. In this case, the interfacial term is ignored. For large χ ($\chi > 2$), there are two minima, indicating phase separation.

The time evolution of the system is governed by the local chemical potential of the components, which is a diffusion equation, given by [12]

$$\frac{\partial \phi_i}{\partial t} = D\nabla \cdot \left[\phi_i \sum_{j=1}^{N} (\delta_{ij} - \phi_j) \nabla \overline{\mu}_j \right]$$

where D is the diffusivity, δ_{ij} is the Kronecker delta, and $\overline{\mu}_j$ is the non-dimensionalized chemical potential of component i, given by

$$\nabla \overline{\mu}_j = \frac{\delta \overline{F}}{\delta \phi_j} = 1 + \ln \phi_j + \sum_{k=1}^{N} \chi_{jk} (1 + \lambda^2 \nabla^2) \phi_k$$

where $\overline{F} = \int \mathrm{d}^3 \boldsymbol{r} \overline{f}$ is the total free energy density.

To solve this non-linear diffusion equation, we use both the explicit Runge-Kutta method and the seme-implicit time-integration scheme combined with Fourier transformation. The first method is a common way, so we only introduce the second. We first discretized the diffusion equation in time and separated the implicit linear and the explicit non-linear terms following the usual IMEX (implicit-explicit) scheme [13] as

$$\frac{\phi_i^{n+1} - \phi_i^n}{\Delta t} = N_i(\phi_i^n) + L_i(\phi_i^{n+1})$$

where ϕ_i^n is the volume fraction of component i at step n, N_i and L_i are the non-linear and linear part of the right-hand side of the diffusion equation, respectively. Following Ref. [14], we introduce an artificial linear ∇^4 term to stabilize the nonlinear term, given by

$$N_i = D\nabla \cdot \left[\phi_i \sum_{j=1}^{N} (\delta_{ij} - \phi_j)\nabla\overline{\mu}_j\right] + AD\lambda^2\nabla^4\phi_i$$

$$L_i = -AD\lambda^2\nabla^4\phi_i$$

where we set $A = 0.5\max\{\chi_{ij}\}$ to stabilize the non-linear part. To solve this semi-implicit equation, we use Fourier Transform $\tilde{\phi}_i(\boldsymbol{k}) = \int \mathrm{d}^3\boldsymbol{x}\phi_i(\boldsymbol{x})e^{-i\boldsymbol{k}\cdot\boldsymbol{x}}$ and get the final expression of ϕ_i^{n+1} as

$$\tilde{\phi}_i^{n+1} = \frac{\tilde{\phi}_i^n + \tilde{N}_i(\phi_i^n)\Delta t}{1 + AD\lambda^2 k^4 \Delta t}$$

So in the numerical simulation, we use the Fast Fourier Transform (FFT) to convert ϕ_i back and forth between real space and Fourier space representations.

III. Results

In this project, we confine our system in two dimensions with 128^2 grids and keep the number of components being 4, with equal global volume fraction ($\phi_{1,2,3,4} = 0.25$). We first non-dimensionalize the PDE and then set $\overline{D} = 1$, $\overline{\lambda} = 0.45 \times 10^{-2}$, $\mathrm{d}\overline{x} = 1/128$, and $\overline{\delta t} = 0.5\overline{\lambda}^2$. We initialize the system to a homogeneous condition with small random noises. We change $\{\chi_{ij}\}$ to explore different morphologies of the solution. Fig. 2 shows the configuration at 10^6 step using the RK4 and FFT methods, respectively. We can see that the topology of the different phases is identical for the two methods, but the FFT method seems to have less interface as the droplets are rounder than those in the RK4. To verify our observation, we calculate the total free energies and plot them in Fig. 3. It can be seen that the energy decreases more significantly for the RK4 in the beginning, but the FFT leads to a more equilibrated state in the end. We also observe unphysical negative ϕ_i at the beginning of the simulation, but it will become physical and stable finally for both RK4 and FFT methods. The speed of computation is about 310 steps/s for RK4 and 450 steps/s for FFT, computed on a personal computer. This is because RK4 has 4 sub-steps during each step so it is relatively slow, whiel the speed of FFT is satisfactory in Python with the pyFFTW package.

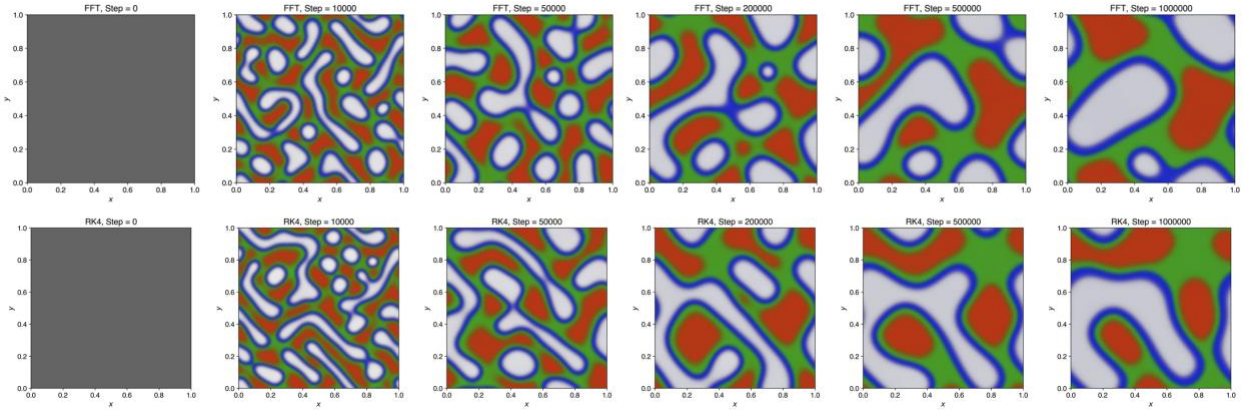

Fig. 2. Simulation configurations of two different methods. The interaction parameters are $\chi_{12} = 2.2, \chi_{13} = 4.6, \chi_{14} = 7, \chi_{23} = 2.2, \chi_{24} = 9.4$, and $\chi_{34} = 2.2$. Components 1, 2, 3, and 4 are colored red, green, blue, and white, respectively.

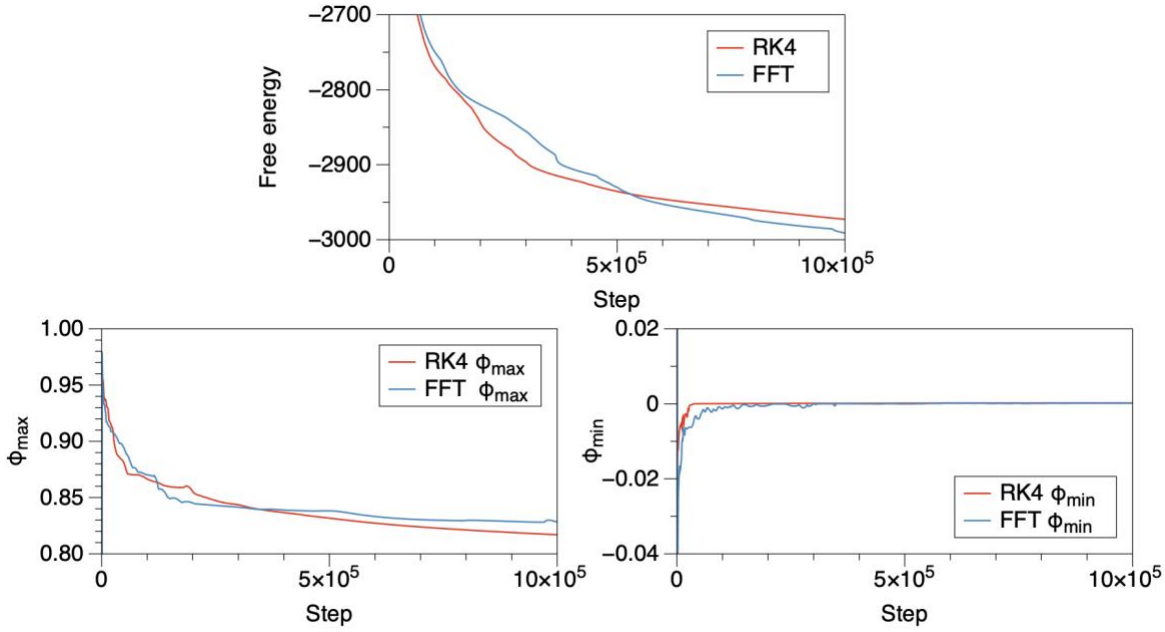

Fig. 3. Output of the above simulations in Fig. 2.

Then we change $\{\chi_{ij}\}$ to explore different morphologies in the multi-component system and compare them with Ref. [15]. Fig. 4 enumerates all results with different phase topologies marked above. As the interaction parameters influence surface tension and the morphology of different phases depends on surface tension, we can realize different morphologies by directly changing $\{\chi_{ij}\}$. Compared with Ref. [15], we find our results are reasonable and physical.

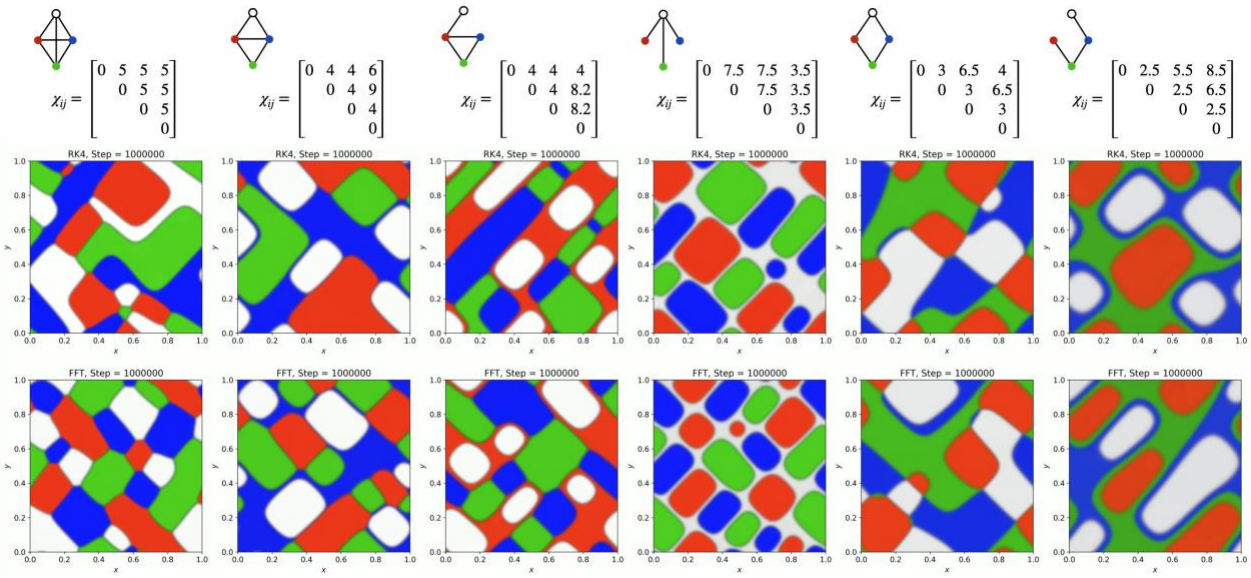

Fig. 4. Simulations of solutions with different phase topologies.

IV. Instruction of code

One needs to install pyfftw package before running the code:

```
$ module load anaconda3/2024.2
(base) $ conda create --name cosmo-env python=3.9 -y
(base) $ conda activate cosmo-env
(cosmo-env) $ pip install pyfftw
```

Then, you can use “sbatch job_della.slurm” to run the simulation. All parameters are specified in file job_della.slurm.

V. References

[1] D. Lohse and X. Zhang, Physicochemical hydrodynamics of droplets out of equilibrium, Nature Reviews Physics 2, 426 (2020).

[2] C. P. Brangwynne, P. Tompa, and R. V. Pappu, Polymer physics of intracellular phase transitions, Nature Physics 11, 899 (2015).

[3] A. A. Hyman, C. A. Weber, and F. J̈ulicher, Liquid-liquid phase separation in biology, Annual review of cell and developmental biology 30, 39 (2014).

[4] S. Boeynaems, S. Alberti, N. L. Fawzi, T. Mittag, M. Polymenidou, F. Rousseau, J. Schymkowitz, J. Shorter, B. Wolozin, L. Van Den Bosch, et al., Protein phase separation: a new phase in cell biology, Trends in cell biology 28, 420 (2018).
[5] C. P. Brangwynne, T. J. Mitchison, and A. A. Hyman, Active liquid-like behavior of nucleoli determines their size and shape in xenopus laevis oocytes, Proceedings of the National Academy of Sciences 108, 4334 (2011).
[6] J. A. Riback, C. D. Katanski, J. L. Kear-Scott, E. V. Pilipenko, A. E. Rojek, T. R. Sosnick, and D. A. Drummond, Stress-triggered phase separation is an adaptive, evolutionarily tuned response, Cell 168, 1028 (2017).
[7] R. Parker and U. Sheth, P bodies and the control of mrna translation and degradation, Molecular cell 25, 635 (2007).
[8] S. F. Banani, H. O. Lee, A. A. Hyman, and M. K. Rosen, Biomolecular condensates: organizers of cellular biochemistry, Nature reviews Molecular cell biology 18, 285 (2017).
[9] Y. Shin and C. P. Brangwynne, Liquid phase condensation in cell physiology and disease, Science 357, eaaf4382 (2017).
[10] R. J. Wheeler and A. A. Hyman, Controlling compartmentalization by non-membrane-bound organelles, Philosophical Transactions of the Royal Society B: Biological Sciences 373, 20170193 (2018).
[11] P. J. Flory, J. Chem. Phys., 1942, 10, 51–61.
[12] P. C. Hohenberg and B. I. Halperin, Rev. Mod. Phys., 1977, 49, 435.
[13] U. M. Ascher, S. J. Ruuth, and R. J. Spiteri, “Implicit-explicit runge-kutta methods for time-dependent partial differential equations,” Appl. Numer. Math. 25, 151–167 (1997).
[14] J. Zhu, L.-Q. Chen, J. Shen, and V. Tikare, “Coarsening kinetics from a variable-mobility cahn-hilliard equation: Application of a semi-implicit fourier spectral method,” Phys. Rev. E 60, 3564–3572 (1999).
[15] S. Mao, D. Kuldinow, M. P. Haataja, and A. Kosmrlj, Phase behavior and morphology of multicomponent liquid mixtures, Soft Matter 15, 1297 (2019).